Simulating Gas-Phase Contamination Distribution In Cleanroom Environments

Authors: Amlan Chakraborty and Jürgen M Lobert – Entegris, Inc.

Entegris

ABSTRACT

Cleanrooms are critical environments for many industries. Contamination control has been a necessity for semiconductor processing for more than 50 years. To maintain ultra-pure air quality in a cleanroom, it is important to understand airborne molecular contamination (AMC) concentrations and air flow profiles throughout the cleanroom and around process tools such as scanners, clean tracks and metrology tools.

A 2-dimensional computational fluid dynamics (CFD) model was developed to understand air flow patterns, concentrations, distribution and mixing of AMC in semiconductor cleanrooms with varying AMC filter coverage for a specific grid of air fan filter units (FFU). The model was utilized to explore the AMC concentration levels and their change for different FFU coverage scenarios at 1st and 2nd pass of air flow.

Model results demonstrate the significant differences in clean and contaminated areas when utilizing less than 100% FFU coverage for AMC filters. We also show significant non-uniformity in air downflow within the cleanroom near process tools, which deflect the laminar air stream. Furthermore, the velocity profiles varied significantly with different height and different positioning of the process tools. That variable flow path created non-uniform, localized concentration increases of AMC in the cleanroom.

The analysis offers insight into AMC concentration and air flow profiles in a cleanroom, and how the contaminant concentrations differ by height and by positioning of the process tools. The study can be used to optimize process conditions, minimize contamination, as well as AMC filter cost of ownership. In addition, the modeling approach employed here can be used to incorporate machine learning, actual AMC measurements, dimensions and cleanroom designs to create a digital twin to simulate the operation, energy budget and contamination control of cleanrooms.

INTRODUCTION

Cleanrooms are critical environments in many industries, such as micro-electronics and pharmaceuticals. Contamination control has been a necessity for semiconductor processing since its beginning more than 50 years ago.[1] Particulate contamination largely follows laminar flow patterns and is easily addressed through filtration with high and ultra efficiency particle filters (HEPA/ULPA). AMC, on the other hand, has become a concern with more sensitive processes, such as deep-UV (DUV) semiconductor patterning around the 90-65 nm technology nodes.[2,3,4,5,6] Over time, cleanroom designs have evolved to minimize impact of AMC, gas-phase chemicals of organic and inorganic nature, typically at parts per billion (ppb, 10^{-9}) level ambient concentrations. AMC is introduced from outside air and from internal sources and dispersed into the cleanroom environment where it can cause damage to process tools, induce defects, and reduce product yield.

In contrast to particulate contamination, AMC does not strictly follow laminar flows. Gas phase contaminants can exhibit substantial lateral diffusion and mixing. If obstacles such as process tools are added to the flow pattern, AMC can be deflected and travel significant horizontal distances to contaminate areas that are traditionally well protected from particulate contamination. To minimize airborne contamination and localize its impact, many cleanrooms are operated under laminar air flow from top down, entering through FFU and exiting through open floors. AMC filters are employed in conjunction with ULPA particle filters on top of FFUs to adsorb AMC. However, laminar flow patterns created by FFU air are often disrupted and altered by the process tools spread out over the cleanroom area. Therefore, to maintain ultra-pure air quality of the cleanroom, it is important to understand AMC concentrations and flow profiles around the process tools.

Such added contamination considerations then require more densely spaced filtration patterns to effectively remove AMC and protect process steps that are sensitive to impact from gas-phase contamination. Understanding flow patterns and AMC distribution can offer key insights to minimize filtration needs, lower cost of operation, while still practicing efficient contamination control – however it's difficult to obtain those by traditional experimentation or by means of analytical methods.

A CFD model can help understand this issue by developing an accurate model. CFD is a modeling technique to create virtual prototypes of real-life systems through the interaction of mathematical equations with underlying physics, which includes fluid flow, heat and mass transport.[7,8,9] In the past, researchers applied CFD models in solving key issues for the design of cleanrooms. Noh et al.[10] predicted particle concentrations and airflow patterns with a goal to improve yield in LCD manufacturing. Thongsri et al.[11,12] tried to understand the airflow and particle distribution around HDD machinery to obtain optimized airflow pattern. CFD modeling was also used to predict contamination in a hospital operating room with the goal to reduce contamination and to develop efficient ventilation systems. Naosungnoen et al.[13] utilized CFD modeling to study airflow and contamination profiles in a manufacturing cleanroom.

EXPERIMENTAL

Objectives

The objective of this study was to develop a numerical CFD model to estimate cleanroom concentrations for organic AMC and flow profiles from AMC filters suspended in an evenly spaced ceiling grid of FFU under varying conditions.

The study simulates air flow patterns and the distribution and mixing of AMC in semiconductor cleanrooms with input parameters being initial AMC concentration, FFU coverage, make-up air percentage and the number of air recirculations. A 2 dimensional cleanroom model was developed with the goal to find average cleanroom AMC concentrations and flow profiles with varying AMC filter coverage on an existing FFU grid, with 0%, 25%, 50%, 75% and 100% of the installed FFUs being equipped with AMC filters. The model further predicts how AMC concentrations and flows are impacted when adding process tools to obstruct the flow path.

The study assumes a simple AMC filter for removal of a specific up-stream concentration. The model is generic and applies to any gas-phase contamination, but we chose toluene to represent the organic AMC class at a concentration of 10 parts per billion (ppb; 10^{-9}) The objective was to find out the average cleanroom concentrations and flow profiles using the following conditions:

1. Vertical cleanroom sizing using a typical semiconductor reference
2. FFUs installed in the ceiling grid, sized and spaced out evenly
3. Removal efficiency of the AMC filter is a constant 90%
4. Initial AMC concentration is 10 ppb
5. AMC filter coverage, evenly spaced out between installed FFUs is 0%, 25%, 50%, 75% or 100%
6. Flow scenarios are one pass only and 2nd pass
7. Make-up (fresh outside) air addition of 15% on each pass, at 10 ppb AMC
8. Addition of process tools, realistically sized to mimic industry standards

Geometry and Computational Domain

The model was developed by the *Ansys Fluent* solver where the mass transfer and fluid flow were governed by Fickian diffusion and Navier Stokes equations. Multiple models were run for each FFU coverage scenario to predict the AMC concentrations and flow profiles in the cleanroom and around the process tools. The model was also employed to indicate AMC concentration levels and their reduction for different FFU coverage scenarios at 1st and 2nd pass.

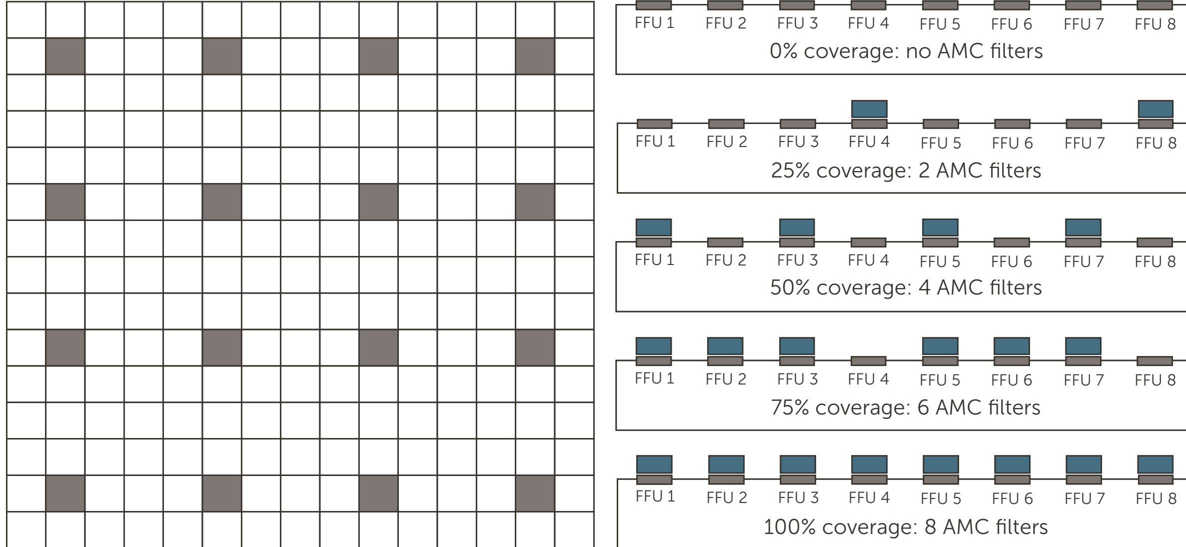

Figure 1. Ceiling grid pattern with 50% AMC filter usage and the five AMC coverage scenarios.

Semiconductor cleanroom ceiling grids typically use 1.2 x 1.2 m (4 x 4 foot) cells, every 4th of which is used for one FFU (Figure 1). All FFUs are used for particle filtration, but only a portion may be used for chemical filtration. The different sub-scenarios we modeled assume five coverage models: 0, 25, 50, 75 and 100% of FFUs used for AMC filtration. Figure 1 shows the top view of a cleanroom ceiling grid of which the shaded blocks are FFUs covered with AMC filters.

Figure 2 shows the three configurations of process tools that are introduced to simulate realistic air flows.

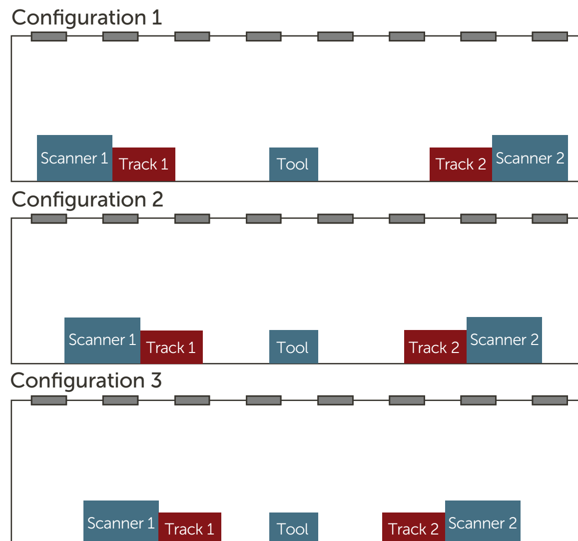

Figure 2. Configurations of process tools with their locations varying relative to FFUs.

Table 1 lists cleanroom specifications, design of FFUs, and operating conditions. The model employed 16000 ceiling grids, but the visual depictions in the figures to follow assume the repetition of the core installation of three tool sets, hence, were limited to the smallest necessary grid size, which then repeats in the model.

Table 1. Parameters for the Ceiling Grid Definition

Parameter	Value
Number of ceiling grids	16000
Each ceiling grids	1.2 x 1.2 m
AMC filter size	0.6 x 0.6 m (2x2 ft)
FFU size	1.2 x 1.2 m
Gap between FFUs	3.6 m
Cleanroom (CR) height	5.5 m / 18 ft
Inlet velocity of AMC filter	1 ms-1
Inlet velocity of FFU	0.258 ms-1
Inlet AMC concentration	10 ppb

Model Assumptions

For our numerical model, the air flow is assumed as Newtonian and incompressible. For the cleanroom operation, we assumed the use of a single-layer chemical filter using activated carbon adsorbent for the removal of organic AMC. Real-world filters may employ other adsorbents to remove other contaminant types, in addition to activated carbon, or multiple layers of adsorbents. Each chemical filter was assumed to have an initial (and constant) removal efficiency of 90%. The removal efficiency of an AMC filter is defined in Equation 1, with [upstream] and [downstream] being the AMC concentrations upstream and downstream of the AMC filter.

$$RE = \left(1 - \frac{[downstream]}{[upstream]}\right) \times 100\ (\%)$$

Equation 1.

As a proxy for organic AMC, we used toluene, a common chemical standard used for semiconductor cleanroom analysis. Toluene concentration was set to 10 ppb upstream of the FFUs, a concentration that is realistic, but at the high-end of state-of-the-art SEMI cleanrooms, low for other industrial settings.

To keep oxygen levels constant and minimize accumulation of carbon dioxide and other non-filtered contaminants, semiconductor cleanrooms operate by partially replacing the recirculated and filtered air with fresh ("make-up") air from the outside of the facility, while some recirculated air is vented to the outside. This portion is typically in the 10-20% range and we assumed 15% make-up air and discharge. We assumed again an average concentration of 10 ppb for that fresh outside make-up air, which, in the real world, is highly variable and can be many times that concentration, depending on local and regional contamination sources and wind direction.

Governing Transport Equations – Continuity

The general continuity equation for dynamic flow includes gas compressibility and an adsorption sink is

$$\frac{\partial(\rho_f)}{\partial t} + \nabla\left(\rho_f \vec{v}\right) = 0$$

Equation 2.

Where ρ_f = gas density (kg/m³).

Governing Transport Equations – Momentum

The airflow is assumed as Newtonian and the momentum equations (Navier Stokes equations) are:

$$\frac{\partial}{\partial t}(\rho_f \vec{v}) + \nabla.(\rho_f \vec{v}\vec{v}) = \nabla p + \nabla.(\bar{\bar{\tau}}) + \rho_f \vec{g} + \vec{F}$$

Equation 3.

Where $\vec{v}$ = gas velocity (m/s), p = pressure (Pa), $\bar{\bar{\tau}}$ = stress tensor, $\rho_f\ \vec{g}\ and\ \vec{F}$ are gravitational body force and external body force, which arise from interactions with the dispersed phase. $\vec{F}$ also contains other model dependent source terms, such as porous media and user defined sources.

The stress tensor is given by:

$$\bar{\bar{\tau}} = \mu\left[(\nabla\vec{v} + \nabla\vec{v}^T) - \frac{2}{3}\nabla.\vec{v}I\right]$$

Equation 4.

Where μ is the molecular viscosity, I is the unit tensor.

Species Mass Balance

In solving the conservation equation of chemical species, *Ansys Fluent* predicts a local mass fraction of each species through a convection-diffusion equation:

$$\frac{\partial}{\partial t}(\rho_f Y_i) + \nabla.(\rho_f \vec{v} Y_i) = \nabla.\vec{J_i} + R_i + S_i$$

Equation 5.

Where R_i is the net rate of production of species i by chemical reaction, and S_i is the rate of creation by addition from the dispersed phase.

Ansys Fluent uses Fick's 1st law to model mass diffusion due to a concertation gradient, which can be written as:

$$\vec{J_i} = -\rho_f D_{i,m}\nabla Y_i - D_{T,i}\frac{\nabla T}{T}$$

Equation 6.

Where $D_{i,m}$ is the mass diffusion coefficient for species i, and $D_{T,i}$ is the thermal diffusion coefficient (Soret effect).

Energy Balance

Figure 7 is the standard energy balance equation.

$$\frac{\partial}{\partial t}(\rho_f E) + \nabla.\left(\vec{v}(\rho_f E + p)\right) = \nabla.\left(k_{eff}\nabla T - \sum_j h_i\vec{J_i} + (\overline{\overline{\tau_{eff}}}.\vec{v})\right) + S_h$$

Equation 7.

Where k_{eff} is the effective conductivity, $\bar{\bar{J_j}}$ is diffusion flux of species j. The first three terms represent the energy transfer due to conduction, species diffusion and viscous dissipation, respectively. S_h indicates the heat of chemical reaction and other volumetric heat sources.

Turbulence Model

Although *Ansys Fluent* offers a number of turbulence models, we selected the Shear Stress Transport (SST) *k-ω* model based on the current flow condition and due to its robust and accurate formulation. The SST *k-ω* model is similar to a standard *k-ω* model but offers the following advantages:

- The SST model incorporates a damped cross-diffusion derivative term in the ω equation
- Turbulent viscosity is modified to transport of the turbulent shear stress

Those refinements make the SST *k-ω* model more accurate and reliable for a wide range of flows than the standard model. The transport equation of the SST *k-ω* model is expressed as follows:

$$\frac{\partial}{\partial t}(\rho_f k) + \frac{\partial}{\partial x_i}(\rho_f k u_i) = \frac{\partial}{\partial x_i}\left(\Gamma_k \frac{\partial k}{\partial x_j}\right) + G_k - Y_k + S_k$$

Equation 8.

and

$$\frac{\partial}{\partial t}(\rho_f \omega) + \frac{\partial}{\partial x_j}(\rho_f \omega u_j) = \frac{\partial}{\partial x_j}\left(\Gamma_\omega \frac{\partial \omega}{\partial x_j}\right) + G_\omega - Y_\omega + D_\omega + S_\omega$$

Equation 9.

Where G_k represents the production of turbulent kinetic energy, G_ω represents the generation of ω. Γ_k and Γ_ω represent the effective diffusivity of k and ω. Y_k and Y_ω represent the dissipation of k and ω due to turbulence.

Modeling Approach

A 2D planar model of the cleanroom including the FFU setup (Figure 2) was developed in ANSYS Gambit and meshed thereafter using tetrahedral cells. The advantage of having a 2D model is that it offers a relatively simple model, substantially reducing computational time. However, it still offers results that compare well to a full 3D model. The mesh was refined accordingly, to achieve a good solution convergence, reduce discretization errors, with a goal to achieve high accuracy.

The model then was exported to *Ansys Fluent* solver to obtain the cleanroom flow behavior and subsequent species transport. The computational cells of the domain are refined enough to obtain maximum convergence (as represented in Figure 2).

In the second part, the models were extended to understand the air flow and contaminant concentration behaviors in the cleanroom along with different metrology tools such as scanners and tracks. The model mesh elements were refined to obtain accurate convergence level.

The incoming air flow is fully turbulent and SST k-ω model was chosen to properly track the turbulence based on flow conditions. The flow path was governed by classical Navier Stokes equations (Equation 3 and 4). The lateral diffusion of contaminants in the cleanroom was accurately estimated by Fickian diffusion in species transport model (Equations 5 and 6). The turbulence model was explained in equations 8 and 9.

As a foundation for the fluid dynamics model, we established the flow scenario where each FFU was assumed to provide 100% of a nominal flow across its 1.2 × 1.2 m dimensions, which translates to a linear velocity of 1 m s^{-1} through one AMC filter of 0.6 × 0.6 m size, sitting on top of an FFU. This flow then presumably travels straight down along laminar flow patterns through an open floor grid into the subfab.

RESULTS

We used the model for a simplified cleanroom environment and staged the capability into several cases.

Velocity Profiles

Assuming minimal flow between FFUs and scaling the FFU flow to the entire floor dimensions, the mass weighted, average flows at different heights are given in Figure 3. The nature of the downstream velocity distribution from each FFU is uniform as expected. However, there are some lateral flow dispersions as flow travels from top to bottom, and the magnitude of the flow gradually reduces due to convection. Figure 3 indicates that the velocity is highest near the top of the cleanroom, and gradually decreases as the flow travels downward. The analysis is particularly useful because the modeling can predict the specific velocity at any specific height in the cleanroom.

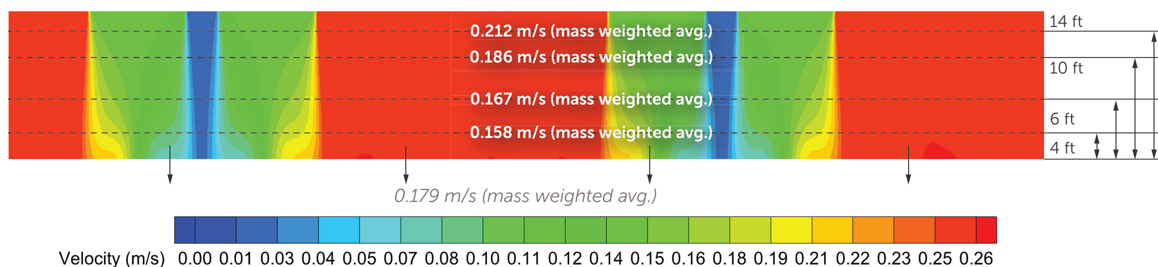

Figure 3. Velocity profile of the cleanroom based on FFU contributions and an open floor grid.

Case 1: First Air Pass Filter Performance with Varying Ceiling Filter Coverage

For the first case of the model, we assumed a constant contamination level and a single pass of air through the FFUs and AMC filters. The AMC filters are assumed to have a constant 90% removal efficiency of the 10 ppb contamination and without any make-up air being added, the resulting concentration profiles from laminar flow through an empty cleanroom are straight forward.

Figure 4 shows the five scenarios predicting AMC concentrations with 0, 25, 50, 75, and 100% filter coverage. Concentration distribution follows the Fickian diffusion model and exhibits significant lateral mixing and dispersion, which was a function of flow velocity and concentration driving force. For the case with no AMC filters (Figure 4a), no contaminants are removed, the cleanroom domain is displayed in red, the entire domain was flooded with maximum contaminant concentration of 10 ppb.

With 25% FFU coverage (Figure 4b), the filters capture 90% of AMC contaminants at 25% of total FFUs. As a result, concentration profiles vary across the clean-room, with air right underneath the FFUs being clean (blue), and large portions still being contaminated (red), air between FFUs gradually mixing (green and yellow). Scenarios with 50 and 75% coverage provide results between those two scenarios.

With very low AMC filter coverage on existing FFUs, the original high contamination level was retained in much of the cleanroom. Only with 75% coverage, the cleanroom started to show effectively filtered air in about half of its space (Figure 4d). To achieve a contamination-free cleanroom, all FFUs need to be covered with AMC filters, to avoid contamination pockets (Figure 4e).

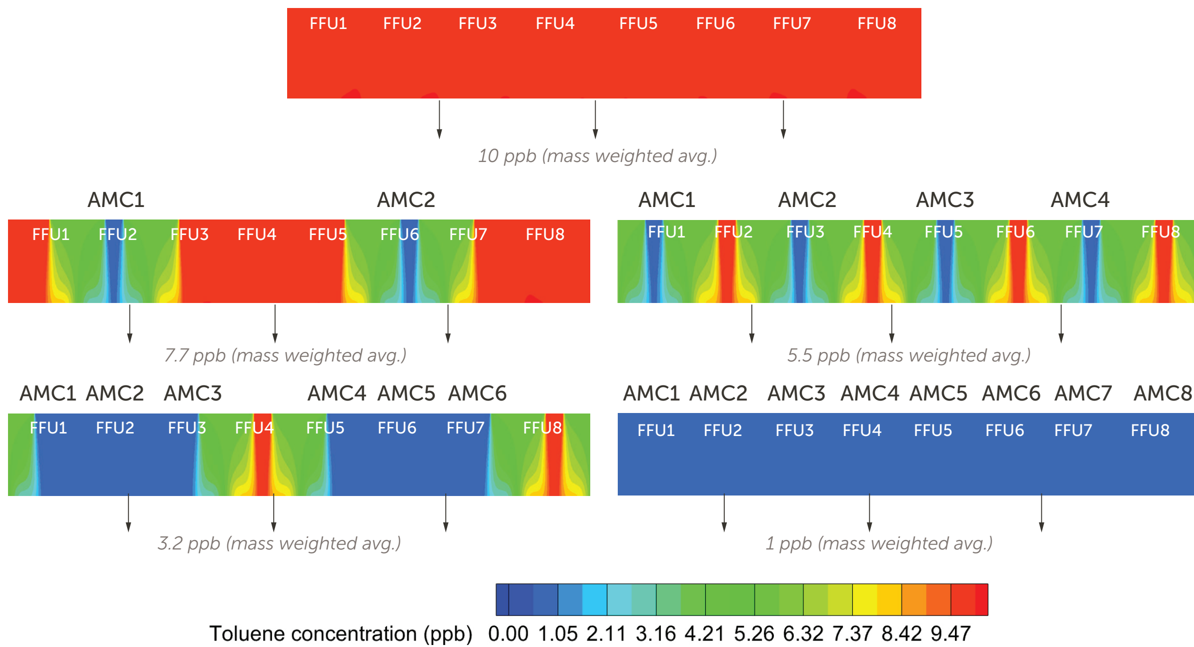

Figure 4. Toluene concentration profiles in an empty, laminar flow cleanroom on first pass and without make-up air. Panels a, b, c, d, and e are scenarios with 0, 25, 50, 75, and 100% FFU coverage of AMC filters. The last panel provides the color scale for the graphs.

The overall, average cleanroom concentration was reduced from 10 ppb to 7.7 ppb near the cleanroom floor with 25% coverage 5.5 ppb with 50% coverage, 3.2 ppb with 75% coverage and about 1 ppb with 100% coverage near the cleanroom floor.

Case 2: Steady-State Filter Performance with Added Make-up Air

For case 2, we introduced 15% make-up air that is contaminated with 10 ppb of AMC and assumed a steady-state recirculating air going through the filters on multiple passes (Figure 5). Despite the added make-up air, which continuously introduced 15% contaminated air into the stream, the air between actively AMC filtered FFUs was now less contaminated compared to the prior case, because of the continuous recirculation.

By introducing recirculation of air, the entire cleanroom gets at least somewhat cleaned up, no part of the cleanroom showed the original 10 ppb concentration anywhere and with 75% FFU coverage, AMC is being removed by at least 50%.

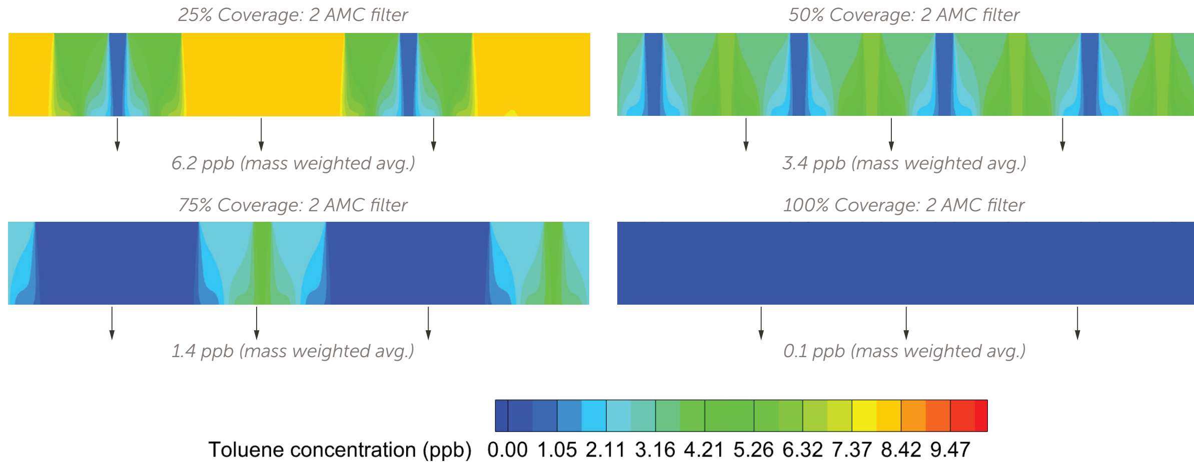

Figure 5. Resulting cleanroom concentrations with recirculation and 15% make-up air being added. Panels a (25% coverage), b (50% coverage), c (75% coverage), and d (100% coverage). The last panel is the color scale.

Table 2 tabulates the average AMC concentrations for the cleanroom and AMC filters operating at 90% removal efficiency. The model predicts that there are 23%, 45%, 68%, and 90% improvements in contaminant reductions for 25, 50, 75, and 100% FFU coverage, respectively, for the 1st pass. The results also clearly demonstrate that a 2nd pass significantly improves the indoor air quality.

Table 2. Average Cleanroom Concentrations for 1st and 2nd Pass of Air Through the AMC Filter

	1st PASS			2nd PASS		
FFU Coverage	**Upstream AMC**	**CR Concentration**	**Improvement**	**Upstream AMC**	**CR Concentration**	**Improvement**
%	ppb	ppb	%	ppb	ppb	%
0	10	10	0	10	10	0
25	10	7.7	23	8.0	6.2	38
50	10	5.5	45	6.1	3.4	67
75	10	3.2	68	4.2	1.4	86
100	10	1.0	90	2.3	0.2	99

Case 3: First Pass Filter Performance with Added Process Tools

The next step in simulating cleanroom concentration profiles was to introduce some process tools. For a simplified approach, we assumed two lithography bay clusters of a scanner and a clean track, plus one stand-alone process tool. We assumed realistic sizing for these tools and then varied their locations relative to the FFUs. Three different tool setup configurations were shown in Figure 2.

Flow Profiles

Figure 6 shows the resulting flow profiles and the associated non-uniformity. Laminar flows get substantially deflected by the added tools. The black lines in each panel are the cleanroom-internal flow swirls between laminar FFU outputs. Whereas those happened without any tools, they get more confined in the flows deflected by tools.

Further, velocity profiles at various cleanroom heights were significantly different for the three configurations (Figure 7). The velocity at different heights behaved in opposite ways if compared to obstructed and unobstructed flow. With the presence of tools, the velocities were nearly constant but higher up to 2 m above the cleanroom floor. That was due to the fact that covering up parts of the floor restricts air flow, which then results in higher exit velocities of about 0.25 m s^{-1}, compared to the 0.18 m s^{-1} for the unobstructed flow. That could be beneficial for flushing out spaces between tools, but we will show that these combined flow paths will have negative consequences on AMC concentrations.

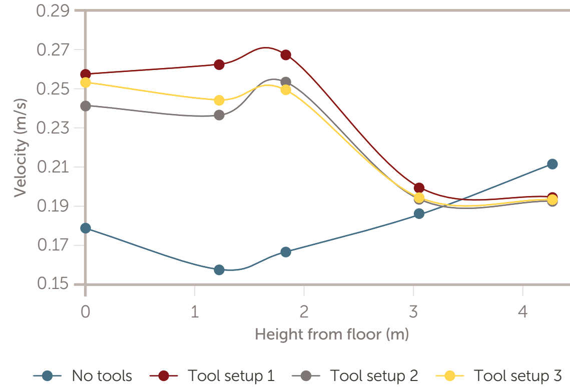

Figure 7. Velocity at different cleanroom heights with four different configurations of metrology tools.

Concentration Profiles

Figure 8 compiles a comparative analysis of AMC concentration profiles in the modeled cleanroom for unobstructed flow versus obstructed flow. As expected, the model contours for the configurations with cleanroom tools are very different from those without tools.

For configurations with tools, the ceiling FFU coverage no longer determines the contamination level at the floor underneath any one FFU. The existence and spatial distribution of the tools creates floor spaces that are heavily contaminated, despite the over-head filtration. All three tool scenarios create such contaminated spaces between the litho clusters and the single tool, as well as areas, where the clean air from the filtered FFUs is confined above the tools, but never reaches the floor.

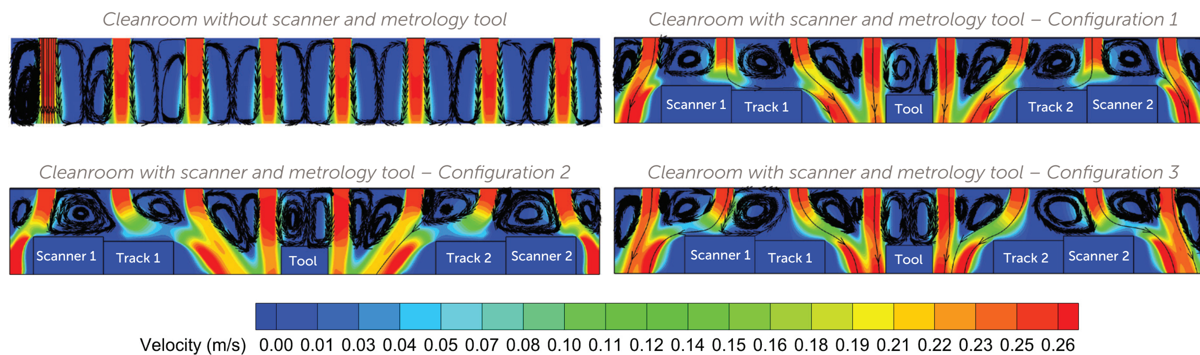

Figure 6. Flow profiles in the modeled cleanroom with different configurations of metrology tools.

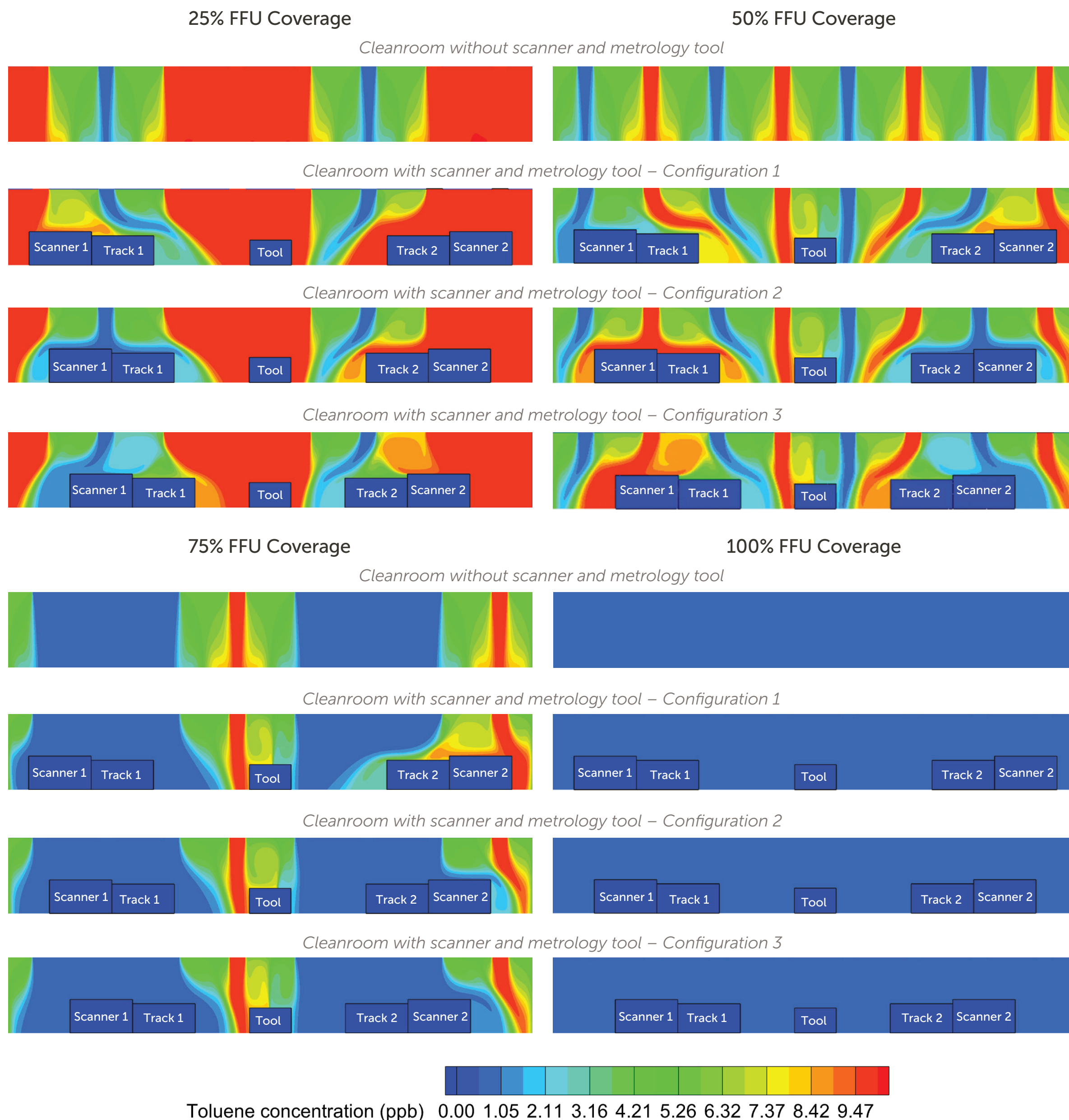

Figure 8. AMC concentrations as a function of FFU coverage around process tools.

Figure 9 is an analysis of concentration profiles of the four tool configurations at different cleanroom heights. The configuration of the tools along the floor significantly determines the uniformity of the concentration profiles above the floor.

Both scenarios for 25% and 75% FFU coverage show substantial (~5%) variability in AMC concentrations compared to the empty cleanroom, whereas the scenario for 50% coverage showed virtually no variability. The exact tool setup along with floor vent coverage in the cleanroom will determine that variability.

Taking these mass weighted average concentration and velocity profiles at different cleanroom heights into consideration could be very useful for cleanroom layout designs. For instance, configuration 2 was the most suitable design from the aspect of lower contaminant concentration variance at any height. This model could help with cleanroom layout to optimize contamination control.

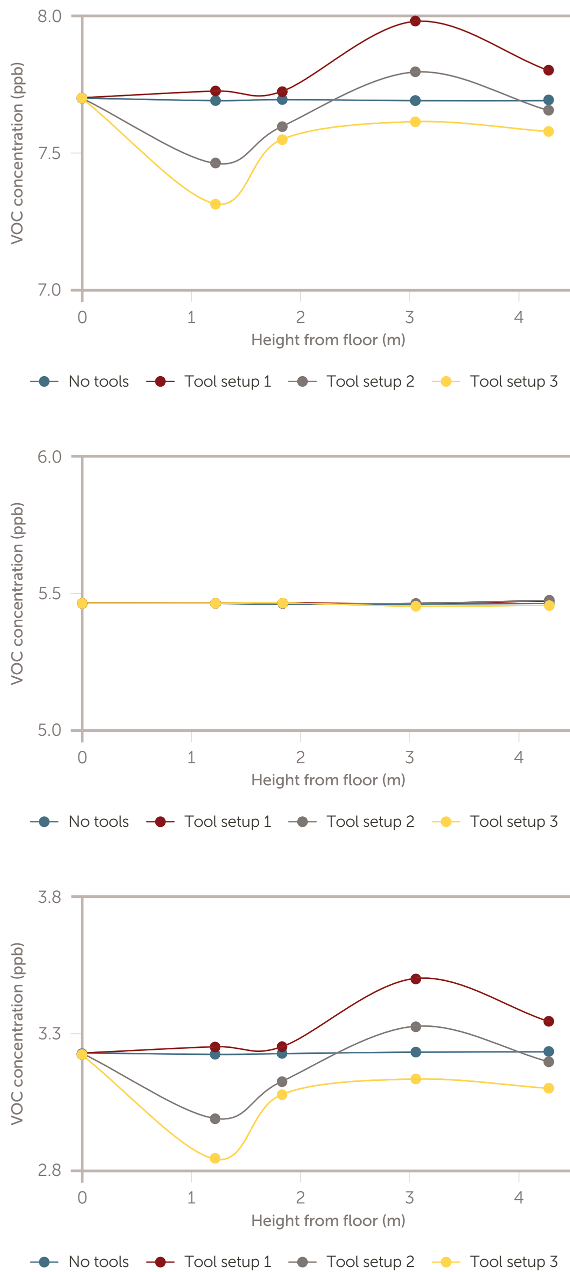

Figure 9. Concentration profiles for the cleanroom with metrology tools for 25% FFU coverage (top), 50% (center), and 75% (bottom).

Model Limitations

The numerical model employed here was purposely limited to a 2-dimensional space, a cross-section of a fictional cleanroom to minimize the computational effort. However, we believe that the results of this 2D model accurately reflect a 3-dimensional cleanroom, because FFU patterns are evenly propagated in the third dimension, so are tool setups in many cleanrooms. Cleanroom dimensions as well as tool dimensions were approximated from real-world objects, but are only representative. The flow was assumed to be incompressible and in an isothermal state.

Chemical filter removal efficiency was assumed to be constant, but, in reality, diminishes over time, along a non-linear curve. AMC filters are typically considered exhausted for practical purposes when they arrive at 80 to 30% removal efficiency, depending on application (50% being common for cleanroom filtration). The chemical and physical adsorption of contaminants were considered out of the scope of the study. Both could be added for a more advanced version.

AMC concentration was set to a fixed 10 parts per billion for simplicity of a decimal base result. That concentration is representative of what we find in modern semiconductor fabs, but actual concentrations vary daily and perhaps hourly and only average at a value close to our assumption.

We assumed an open floor grid for the entire cleanroom, which assists in venting the flow patterns from the FFUs. In reality, there is a limited number of open spaces in the floor, parts of the floor may be obstructed by tubes and installations underneath the grid, and some cleanrooms only have limited openings every few meters apart, rather than a truly open floor grid. This was not considered and would make flow distribution less uniform, resulting in more contamination at the floor level in certain spaces.

Finally, the color scale shown does not allow to visualize small differences in concentration, such as those expected between FFUs at the ceiling, a space that is not readily flushed out quickly or ever. Those differences exist and can be calculated, but do not show in the figures provided here.

CONCLUSIONS

Our numerical model analysis explores the improvement of air quality in a simulated semiconductor cleanroom with and without process tools for different FFU coverages with AMC filters. It also analyzes the air flow and contaminant concentrations profiles at different heights of the cleanroom. The model further explored how flow and concentrations were affected by various configurations of process tools. The model is a valuable tool for the optimization of contamination control.

For clarity and simplicity, we limited the model to a 2-dimensional cross-section of a fictional cleanroom. However, the model capability could easily be expanded to three dimensions, along with actual cleanroom dimensions, ceiling fan configurations and tool sizes / placement to digitally duplicate a real-world industrial setting that can be used for contamination control, cost optimization as well as energy modeling. Such a model should also be fine-tuned by considering the actual floor exhaust design to achieve most realistic flow paths and impact areas.

Further refinement could add contamination sources other than ceiling entrainment such as tool exhaust and human presence, and be cross-checked with measured variability of AMC concentrations, perhaps assisted by machine learning. The model could then become a digital twin for that environment. With such a digital twin, any change in flow patterns or contamination could then be predicted for every change in cleanroom layout or the addition or removal of process tools.

Given the highly variable nature of ambient air pollution, as well as differences in cleanroom sections, the model can be further optimized by monitoring AMC concentrations, as well as AMC filter performance, to yield an optimized cost of ownership and maximized cleanroom protection.[14]

This technical paper was presented by Amlan Chakraborty and Jürgen M Lobert at FILTECH 2023 in Cologne, Germany, February 14-16, 2023.

References

1. Federal Supply Service, FED-STD-209, Federal Standard cleanroom and workstations requirements, controlled environment. 1963.

2. DIN EN 1822-1:2019 standard on: High efficiency air filters (EPA, HEPA and ULPA) – Part 1: Classification, performance testing, marking.

3. John K. Higley and Michael A. Joffe, "Airborne Molecular Contamination: Cleanroom Control Strategies", Solid State Technology, pp. 211, July 1996.

4. Devon Kinkead and Monique Ercken., "Progress in Qualifying and Quantifying the Airborne Base Sensitivity of Modern Chemically Amplified DUV Photoresists," Proceedings, Vol 3999, Advances in Resist Technology and Processing XVII; https://doi.org/10.1117/12.388362, 2000.

5. Mats Ekberg et al., "Airborne Molecular Contamination Control in the Micromirror SLM-Based Deep Ultraviolet DUV SIGMA7300 Laser Pattern Generator", Proc. SPIE, vol. 5377, Optical Microlithography XVII, (28 May 2004); https://doi.org/10.1117/12.535833.

6. Jitze Stienstra, Joseph Wildgoose, Jürgen Lobert, Christopher Vroman, and David Ruede, "A 21st Century Approach to Airborne Molecular Contamination Control", Gases & Instrumentation, Vol. 4-2, 12-15, 2010.

7. K. Rambabu, L. Muruganandam, S. Velu, CFD simulation for separation of carbon dioxide-methane mixture by pressure swing adsorption, Int. J. Chem. Eng. 2014 (2014). https://doi.org/10.1155/2014/402756.

8. A. Chakraborty, S. Kumar, Thermal management and desorption modeling of a cryo-adsorbent hydrogen storage system, Int. J. Hydrogen Energy. 38 (2013) 3973–3986.

9. A. Chakraborty, J. Cook, R. Gipson, Parametric Optimization of Gas Purifiers: A Computational Fluid Dynamics (CFD) Modeling Approach, in: IEEE - ASMC, 2019. https://doi.org/978-1-5386-7601-1/19.

10. K.C. H. Noh, H. S. Kim, and M. D. Oh, "Study on contamination control in a minienvironment inside cleanroom for yield enhancement based on particle concentration measurement and airflow CFD simulation," Building and Environment, vol. 45 , pp. 825-831, 2010.

11. J. Thongsri and M. Pimsarn, "Optimum airflow to reduce particle contamination inside welding automation machine of Hard Disk Drive production line," International journal of precision engineering and manufacturing, vol. 16, no. 3, pp. 509-515, 2015.

12. J. Thongsri and A. Khaokom, "Successful simulation of airflow in the microenvironment of an assembly automation machine and its implication," Advanced Materials Research, Vol. 931-932, 1063-1067, 2014.

13. J. Naosungneon and J. Thongsri, "Simulation of airflow in a cleanroom to solve contamination problem in an HDD production line" International Journal of Mechanical Engineering and Robotics Research, Vol. 7, No. 1, pp. 41-45, 2018.

14. Jürgen M Lobert and Joseph R Wildgoose. Optimizing Semiconductor HVAC Filtration. Gases & Instrumentation, Vol. 20-23, May/June 2009. Online article.

FOR MORE INFORMATION

Please call your Regional Customer Service Center today to learn what Entegris can do for you.
Visit entegris.com and select the Contact Us link to find the customer service center nearest you.

CONTENT AND LIABILITY DISCLAIMER

Entegris believes the information in this document is accurate as of its publication date. Any and all specifications and designs are subject to change without notice. Entegris is not liable for errors or omissions in this document. Entegris undertakes no obligation to update the information presented in this document. You may not use or facilitate the use of this document in connection with any infringement or other legal analysis concerning Entegris products described herein. You agree to grant Entegris a non-exclusive, royalty-free license to any patent claim thereafter drafted which includes subject matter disclosed herein. No license, express or implied, by estoppel or otherwise, to any intellectual property rights is granted by this document.

Corporate Headquarters
129 Concord Road
Billerica, MA 01821
USA

Customer Service
Tel +1 952 556 4181
Fax +1 952 556 8022
Toll Free 800 394 4083

Entegris®, the Entegris Rings Design®, and other product names are trademarks of Entegris, Inc. as listed on entegris.com/trademarks. All third-party product names, logos, and company names are trademarks or registered trademarks of their respective owners. Use of them does not imply any affiliation, sponsorship, or endorsement by the trademark owner.

©2024 Entegris, Inc. | All rights reserved. | Printed in the USA | 9000-13589ENT-0524